Ethiopian Journal of Water Science and Technology (EJWST)

DOI: https://doi.org/10.59122/EJWST777

Vol. 9, 2026, Pages: 32~60 ISSN (Print): 2220-7643

Synchronizing Time Series Satellite Data and Field Data Measurement to Assess Sedimentation in Koka Reservoir of Ethiopia

Tafesse Fitensa Disasa[1], Abebe Temesgen Ayalew[2*], Dereje Teferi Gizachew[1], Mengistu Regassa Batu[1] , Geleta Guta Nigus[1]

[1]Faculty of Water Resources and Irrigation Engineering, Arba Minch Water Technology Institute, Arba Minch University, Ethiopia
[2]Faculty of Hydraulic and Water Resources Engineering, Arba Minch Water Technology Institute, Arba Minch University, Ethiopia
Corresponding Author*: Abebe Temesgen Ayalew; abebe.temesgen@amu.edu.et; Scopus Author ID: 57406817400

ABSTRACT

Regular reservoir surveys are necessary to assess the reduction in storage capacity caused by sediment deposition. Optimal water allocation requires up-to-date information on reservoir storage and sedimentation status, yet such information is often limited. This research is aimed at assessing the sedimentation of Koka Reservoir by integrating time series satellite image data (25-day satellite image data) and real-time reservoir water measurements with 20 years of average discharge and 25 days of reservoir level. The reservoir surface area was extracted from satellite images using QGIS, aided by Automated Water Extraction Index (AWEI) to identify water pixels. Water level records from the reservoir gauging station were combined with surface area to estimate reservoir volume using a prismoidal formula. The resulting estimates were used to update the elevation-capacity curve. The findings showed that the current storage capacity at full reservoir level is 780.01 Mm^3. This indicated that 869.99 Mm^3 of silt had been accumulated in the reservoir since initial operation. This corresponded to a loss of approximately 52.73% of the original storage capacity. The mean annual sediment deposition rate over the 62 years of operation was 14.03 Mm^3, equivalent to an annual sedimentation rate of 0.85%. This rate was comparable to the global index of annual reservoir sedimentation which ranged between 0.5% and 1%. The research findings provided up-to-date information of sedimentation status at Koka. These results could support informed water allocation planning for effective reservoir water management. Scheduling sediment flushing during the peak flood periods of the upper Awash River can provide an adaptive approach to managing sedimentation in the Koka Reservoir.

Keywords: Elevation-capacity curve, Koka reservoir, Reservoir sedimentation, Sediment deposition rate, Time-series satellite data

Received: 25 Novmeber, 2025; Accepted: 01 January, 2026 Published: 04 May 2026

1 INTRODUCTION

Reservoir sedimentation is a gradual accumulation of soil, sand, and debris from watersheds, reducing water storage capacity by 0.5%–1.0% annually worldwide (Prasad et al., 2018). Global reservoir storage capacity has been shrinking due to sediment inflow exceeding new construction since 2006. The process poses a significant threat to water security, costing an estimated $13-20 billion annually in lost capacity (Garg et al., 2020). Reservoir sedimentation is a critical issue across Africa as dams lose 0.5%–1% of their storage capacity annually. Particularly in the Ethiopian Highlands and East Africa, dams face up to 3%–16% annual loss (Chamoun et al., 2016). This rapid accumulation of sediment, driven by soil erosion and climate change, severely limits water storage for hydropower, irrigation, and consumption.

Sedimentation is a critical issue for reservoirs in Ethiopia, particularly in the highlands, causing significant loss of storage capacity for water supply, irrigation, and hydropower. High erosion rates in watersheds lead to annual capacity losses of 1.7% to 16.2% in small reservoirs, with notable examples like the Koka Dam (43.2% loss in 63 years) and Angereb Reservoir (62.28% loss in 16 years) (Adugna & Cherie, 2021). Reservoirs are water bodies created by constructing dams across rivers to store significant volumes of water for different purposes. They play essential roles in water management by altering spatial and temporal storage of surface runoff (Zhou et al., 2016). However, deposits of sedimentation in those reservoirs affect the intended function of reservoirs.

Sediment deposit in reservoirs is the process by which sediment particles are transported by river flow and progressively built up in the reservoir (Wagh & Manekar, 2021). Ultimately, huge quantities of sediments accumulate behind a dam owing to the velocity of water entering the reservoir (Prasad et al., 2018). The reduction of flow velocity reduces transportation capacity of sediment and leads to deposition of sediment on reservoir bed (Merina et al., 2016).

Sedimentation is an unstoppable phenomenon that diminishes storage capacity, threatens dam safety, reduces energy production, and incurs heavy financial losses (Prasad et al., 2018). Apart from reducing storage capacity, reservoir sedimentation has a negative impact on proper functioning of the outlet structures including bottom outlet and intakes (Chamoun et al., 2016). On top of that, it causes safety and operational issues to the dam reservoir (Garg et al., 2020). The deposition of sediment causes 1% loss of global reservoir storage capacity (Garg et al., 2020). The annual loss of existing reservoirs worldwide is predicted to fall within the range of

0.5 to 1% (Pandey et al., 2016). It has been estimated that about 40,000 dams around the world are losing about 0.5 to 1% of their storage capacity annually (Merina et al., 2016). Likewise, Rahamani et al. (2018) and Singh et al. (2023) in their work indicated that the annual rate of reservoir depletion caused by sedimentation was approximately 0.84% and 0.58% respectively. Like its global challenges, reservoir sedimentation is a critical problem to Ethiopian reservoirs such as Aba Samuel, Gilgel Gibe I, and Angereb, leading to substantial decrease in the original capacity of reservoirs due to larger amounts of deposition than expected (Adugna & Cherie, 2021).

The storage volume of Koka Reservoir is significantly reduced due to excessive accumulation of sediment. The 1999 survey results showed that the available live storage volume of Koka Reservoir was reduced to 1186 Mm^3 from its original capacity of 1650 Mm^3 (Ministry of Water and Energy, 1999). Similarly, the 2015 prediction report stated that the storage capacity of Koka Reservoir was reduced to 978.73 Mm^3, resulting in a 41% loss of its original live storage volume (REACH, 2020). Despite the significant loss of volume owing to sedimentation, water allocation for several downstream areas still relied on this reservoir. Conversely, the increasing demand from downstream users necessitated equitable water allocation. Yet, recent information regarding available reservoir active storage capacity was limited. This increased the level of uncertainty in equitable water allocation and posed a challenge for water resource planners and decision makers closely working on this reservoir. Updating a storage capacity curve through systematic and periodic assessments of reservoir sedimentation is crucial for optimum allocation of the remaining water in the reservoir (Narasayya et al., 2012). The information about the available quantity of water in the live storage zone and sedimentation status in the reservoir is also important for the optimal allocation of water (Mandwar et al., 2013; MupFiga et al., 2016). Assessment of reservoir sedimentation provides information about reservoir capacity, which can be used to modify the reservoir operation schedule for optimal utilization of the remaining water in the live storage zone (Tiwari et al., 2016; Khadatare & Jedhe, 2017; Rai et al., 2019). However, an updated reservoir capacity curve is lacking in developing countries due to limited periodic reservoir sedimentation assessments. Substantial pieces of literature reveal that there are various methods to update reservoir storage capacity curves through systematic reservoir sedimentation assessments. Conventional methods like hydrographic survey are accurate and widely used predictable methods for sedimentation assessment in reservoirs, but they are time-consuming, laborious, risky, and

expensive (Tiwari et al., 2016; Rai et al., 2019; Jeyakanthan et al., 2020). Inflow-outflow analysis is another method that needs an intensive record of sediment data and except its limited application in reservoir sedimentation assessment especially in developing countries owing to the lack of well-developed and frequently monitored sediment sampling stations (MupFiga et al., 2016). Besides, the difficulty of gauging all river tributaries entering reservoirs along with all outlets cannot be ruled out (Sharad & Sanjay, 2011). The use of remote sensing method to assess reservoir sedimentation is becoming increasingly more popular due to the availability of a long-period archive of data with high spatial, spectral, and temporal resolution (Sharad & Sanjay, 2011; Narasayya et al., 2012). Analysis of this repetitive data provides accurate information on the reservoir surface area at a specified elevation, while combining multi-date reservoir areas derived from satellite data enables the computation of reservoir volume. Remote sensing techniques are emerging as superior means to conventional methods for the assessment of reservoir sedimentation due to their recency and reliability (Mandwar et al., 2013), effectiveness in cost and time (MupFiga et al., 2016; Pandey et al., 2016; Tiwari et al., 2016; Jeyakanthan et al., 2020). The remote sensing techniques in the recent decade have been widely used to assess reservoir sedimentation since they provide continuous, cheap, and wide spectral range of data (Shukla et al., 2017; Al Balsmeh et al., 2020), overcome the problems of conventional methods (Prasad et l., 2018),are fast, accurate, and effective in live storage zone (Garg et al., 2020). However, the effectiveness of these methods is limited to the lowest observed water level in the reservoir. Recently, the use of satellite data has been considered as an inexpensive and emerging technique to generate real-time information about reservoir sedimentation.

Sedimentation in the Koka Reservoir involves complex internal hydrodynamic forces driven by the interaction between incoming river flow (Awash River) and the calm standing water of the dam. Key internal physical forces causing sediment deposition include gravity, density currents, and decreased flow velocity resulting in a 43.2% capacity reduction between 1960 and 2023. High-intensity rainfall, combined with erodible soils and steep topography, accelerates the transport of clay and silt particles causing rapid storage loss. Sedimentation in the Koka Reservoir is primarily driven by high soil erosion rates in the upper Awash Basin Catchment exacerbated by rapid land-use changes, deforestation, and unsuitable agricultural practices on steep slopes. However, the literature is limited on studies utilizing remote sensing techniques to evaluate reservoir sedimentation in Ethiopia, especially concerning the Koka

Reservoir. Hence, assessing sedimentation in this reservoir using a time and cost-effective method is important. A novel aspect of this research involves integrating in-situ reservoir level measurements with satellite data archive to extract reservoir surface area during each date of satellite passing over the reservoir. By combining these data sources, this approach offers a unique and accurate method for assessing reservoir sedimentation. Therefore, this research is aimed at updating the elevation-capacity curve from multi-date satellite image analysis; it estimates the loss of reservoir volume in the live storage zone due to sedimentation and the average annual sedimentation rate by integrating remote sensing data and in-situ reservoir water levels. This has considerable significance in providing the limited information about the remaining live storage capacity of the reservoir. It also helps water resource planners and decision-makers ensure robust and equitable water allocation for all users.

2 MATERIALS AND METHODS

2.1 Study area

2.1.1 Location

Koka Reservoir is in the upper Awash Sub-basin of the Awash River Basin of Ethiopia, (Figure 1). The geographical location of this reservoir at the dam outlet is 517091N latitude and 935985E longitude. The upper Awash Sub-basin, which contributes the flow to Koka Reservoir, has a catchment area of about 11,524.9 km^2 (Fitensa et al., 2019). The original Minimum Operating Level (MOL) and Full Reservoir Level (FRL) during its initial operation were at elevations of 100.4m and 110.3m, respectively (Ethiopian Electric Power Corporation 2004).

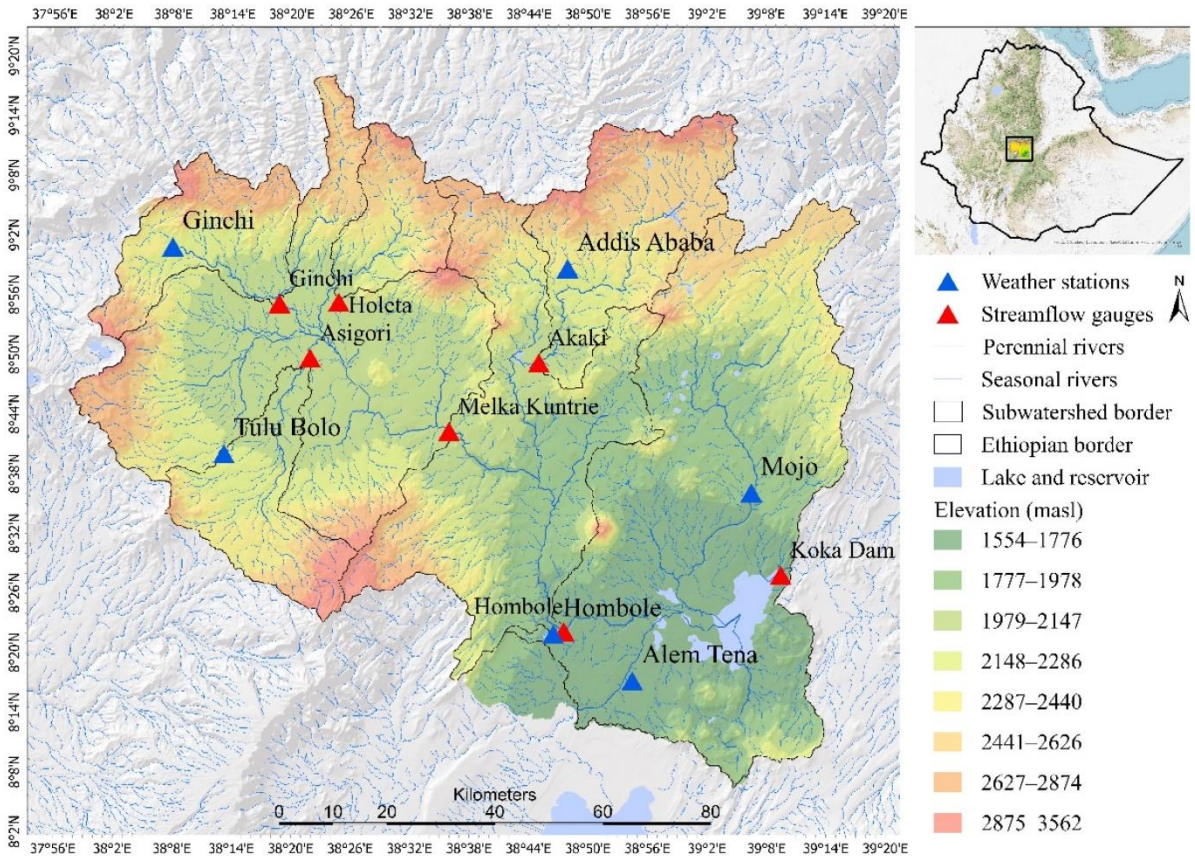

Figure 1. Map of the Upper Awash River Basin.

2.1.2 Silent Features of the Koka Reservoir

The Koka Reservoir has been in operation for over 60 years and serves as a primary water source for downstream users, including domestic water supply for Adama city, irrigation land covering around 64,124 hectares, and power production (REACH, 2020). Previous sedimentation surveys on the reservoir reported that its lifespan was threatened by excessive accumulation of sediment. The first survey attempt was conducted in 1973 and revealed a total volume of 136 Mm^3 sedimentation with an annual silt deposition rate of 10 Mm^3 (Ministry of Water and Energy, 1999). The second survey, conducted in 1981, reported a total silt volume of 350 Mm^3 deposited in the reservoir, resulting in an annual siltation rate of 17 Mm^3. The next attempt in 1988 recorded a total sedimentation volume of 470 Mm^3, with an annual sedimentation rate of 16.8 Mm^3 (Ministry of Water and Energy, 1999). A team from the Ministry of Water and Energy conducted the fourth sedimentation survey in 1999 and reported an annual sedimentation rate of 12.2 Mm^3. Based on earlier surveys, the Awash Basin Authority projected the fifth sedimentation status of the reservoir in 2015. The report indicated

that the average annual sedimentation rate was 13 Mm^3 while the minimum reservoir operating level was raised to 103.6m from its original level of 100.4m (REACH, 2020).

2.2 Data Collection

2.2.1 Field Data

The original reservoir capacity curve of 1959 and the hydrographic survey report of 1999 were provided by the Ministry of Water and Energy (MoWE) while the 2015 sedimentation estimate report was received from Awash Basin Authority (ABA). The 1999 hydrographic survey map was digitized and used to validate the water surface area extracted from the satellite images. Historical data for the Koka Reservoir in Ethiopia is segmented by season specifically the Kiremt (rainy, June-September) and Bega/Belg (dry/short rains, October-May) because of significant fluctuations in inflow and volume. Maximum inflow typically occurs from June to November while minimum storage is reached in July before the main rainy season.

a) Upper Awash Flow Data

Flow data from the Upper Awash at Hombole Station (1990-2011) was obtained to identify the optimal time window for scheduling reservoir sediment flushing.

b) Ground Control Points

The spatiotemporal satellite images of the reservoir area were georeferenced in order to assess the dynamics of reservoir spread by superimposing the images of each date (Shukla et al., 2017). Georeferencing required a minimum of four ground control points (Tawfeik et al., 2016). However, for increased accuracy, more evenly distributed ground control points (GCPs) were considered. Prior to the field visit, a detailed investigation of the study area was carried out to identify appropriate places for collection of GCPs. The satellite acquisition calendar over the area of interest AOI was identified using a path of 168 and a row of 54. Then, Landsat-8 Operational Land Imager (OLI) image was downloaded from the United States Geological Survey (USGS) official website. After careful investigation, land features that were clearly visible from the satellite image, such as the edge of buildings, river bridges, river confluences, and road intersections, were selected as suitable places for GCPs.

To geo-reference the LANDSAT images, a total of 23 spatially well-distributed GCPs were collected from the AOI at selected land features during a field visit using a portable Global Positioning System (GPS). However, to minimize complexity and reduce human-induced

errors, only four GCPs located near the four corners of the AOI were used for georeferencing the satellite images.

c) Topographic Data

One of the crucial steps in satellite image preprocessing involves topographic correction. To achieve this, a 30 m x 30 m resolution Digital Elevation Model (DEM) of the Shuttle Radar Topography Mission (SRTM) was acquired from the USGS official website. The downloaded DEM was used as input for topographic correction during the image preprocessing phase.

d) Reservoir Water Level Data

In-situ water level data corresponding to each satellite overpass were obtained from the Koka Hydroelectric Power Station. A total of 25 days of reservoir level data were collected and used to develop the elevation-storage curve. Real-time water level measurements for the Koka Reservoir were conducted daily to inform operational decisions, particularly for flood control, power generation, and irrigation releases. The data were collected using in-situ gauging stations supplemented by satellite remote sensing (e.g., Sentinel-2) to monitor reservoir levels, inflows (Akaki, Hombole, Melka Kuntrie, Mojo stations), and surface evaporation.

2.2.2 Satellite Data

Nowadays, several satellite sensors collect earth information. The spatial, spatiotemporal, and spectral resolutions of these satellites were crucial for selecting data for analysis. Landsat-8 OLI and Sentinel 2 Multispectral Instrument (MSI) are part of the new generation of satellite sensors known for their medium spatial resolution. Landsat-8 OLI features nine bands with a spatial resolution of 30m except for the PAN band which has a 15m spatial resolution. The spatiotemporal resolution of this sensor is 16 days (United States Geological Survey, 2020).

Conversely, Sentinel 2 MSI has 13 spectral bands with four bands at 10m, six bands at 20m and three bands at 60m spatial resolutions. The Spatiotemporal resolution is also 10 days with one satellite and 5 days with two satellites (European Space Agency, 2020). Sentinel 2 MSI provides images with better spatial, spectral, and spatiotemporal resolution relative to Landsat-8 OLI. However, the footprint of Sentinel takes images of the Koka Reservoir in multi-scenes separated by ten days while Landsat captures the image of the AOI under a single scene every sixteen days. Although a mosaic image of Sentinel can be created to obtain a complete AOI image, the reservoir level within a ten-days period is subject to fluctuation. As a result, Landsat-

8 OLI images were selected for this research. The 25-day image data of Landsat-8 OLI, categorized as collection 1 of Level 1, was downloaded from the USGS.

2.3 Method of Data Analysis

2.3.1 Image Screening

The 25-day satellite image data were not directly used for preprocessing. Screening was done for all downloaded images based on the percentage of cloud cover. After careful investigation of the images, it was decided that images exhibiting a cloud cover lower than 25% could be used for further analysis without introducing significant errors. And, the 16-day images with cloud cover less than 25% were selected for further analysis (Figure 2).

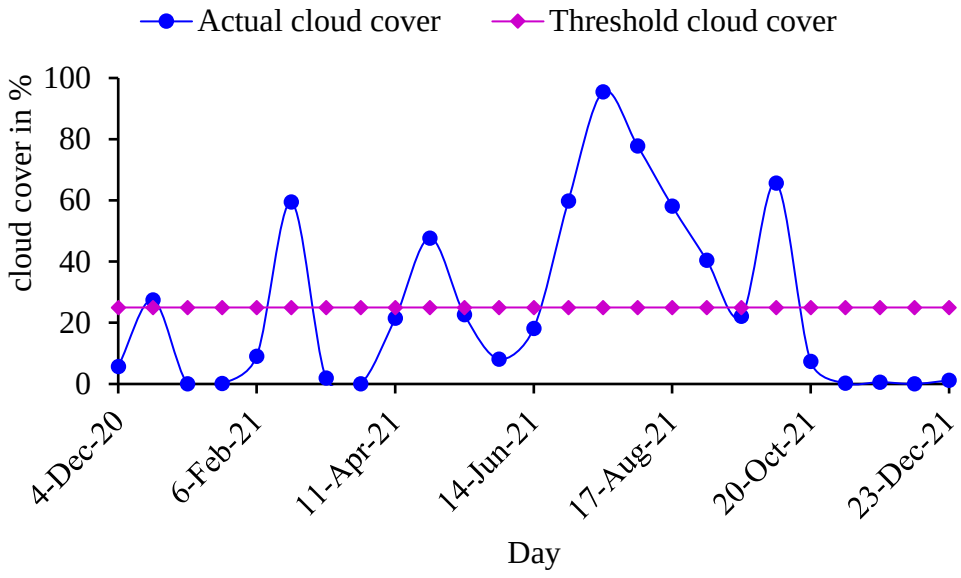

Figure 2 Landsat-8 OLI Image screening based on cloud cover percentage

2.3.2 Identifying Area of Interest

Analysis of the full scene of the Landsat image was time-consuming and required a large storage volume. Hence, only the images of Area of Interest AOI were extracted from the entire scene for preprocessing. The Area of Interest (AOI) was delineated using the following Universal Transverse Mercator (UTM) coordinates: (490,000 E, 950,000 N), (490,000 E, 910,000 N), (530,000 E, 910,000 N), and (530,000 E, 950,000 N).These coordinate values were used to create a polygon shapefile of the AOI. The resulting shapefile served as a mask feature to extract the Landsat image of the AOI from the entire scene.

2.3.3 Band Combination

During georeferencing, pinpointing the location of GCPs on individual band pixels proved challenging. To enhance clear visibility of GCP location on each pixel, a virtual raster of AOI was created using images of band 2 to band 7. The virtual raster was used to create the False Color Composite (FCC) by rendering multiband color so that bands 4, 3 and 2 were displayed on red, green and blue bands respectively. This approach improved the clarity of GCP locations on pixel of individual bands. The FCC image of the AOI was georeferenced using four GCPs selected from the 23 collected during the field survey. This georeferenced FCC image was used as a base image for further georeferencing. All Spatiotemporal images were georeferenced using the base image through image-to-image co-registration (Figure 3).

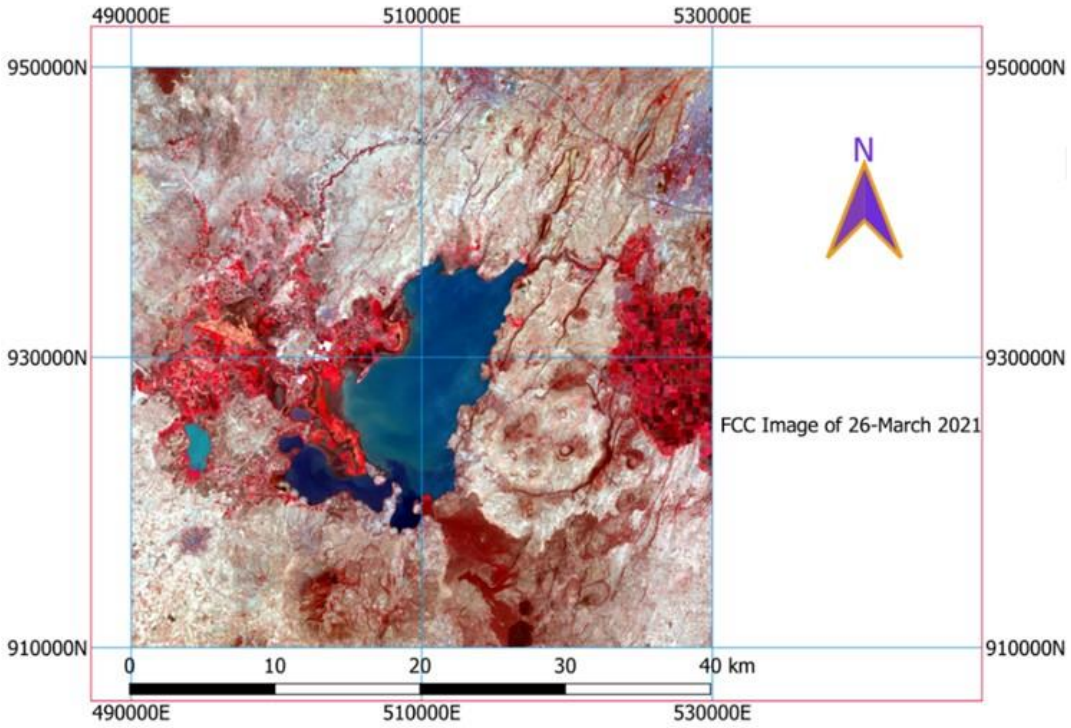

Figure 3 Georeferenced Base Image of AOI

2.3.4 Preprocessing Images of Landsat-8 OLI

The analysis of image data was undertaken using QGIS. Additionally, the Orfeo Toolbox (OTB) and System for Automated Geoscientific Analysis (SAGA-GIS)were integrated into QGIS interface for specific image preprocessing. QGIS, OTB, and SAGA-GIS were powerful combinations for multispectral satellite image analysis. Beyond their open-source nature, the availability of several plugins and functions made this software superior in preprocessing and

post-processing of different satellite images, including the Landsat-8 image. Consequently, QGIS was preferred to perform satellite image analysis.

a) Geometric Correction

Landsat images required preprocessing to minimize distortions caused by sensor, solar, atmospheric, and topographic effects (Young et al., 2017). The geometric correction process involved two separate stages: georeferencing, which involved assigning the actual geographical coordinates to the satellite image. This step aligned the pixels of the satellite image with their true locations on the ground. The second stage was correction for relief and view direction distortions. The georeferenced bands were corrected for relief and view direction distortions through an orthorectification process. This process was executed by calling the OTB within the QGIS interface. The georeferenced individual bands were used as inputs for the orthorectification.

b) Conversion of DN to Physical Quantities

The Landsat Level 1 products can be downloaded in the form of digital numbers (DN). However, using the DN value directly for analysis can generate error as the spectral values of objects on Earth are subject to Spatiotemporal dynamics (Young et al., 2017). In multi-spatiotemporal data sets, a spectral signature that is constant over time may show notable DN variations (Pacifici et al., 2014). Hence, the DN values of all multi-spatiotemporal images should be converted to a common scale such as at-sensor radiance or top-of-atmosphere (TOA) reflectance. To transform DN of the image into a physical quantity, the computation of at-sensor or top-of-atmosphere (TOA) radiance is vital but is rarely used for further image processing. The use of TOA reflectance in relation to TOA radiance has various advantages: These include the elimination of the cosine effect of solar zenith angles, correction for variations in exo-atmospheric solar irradiance, and adjustment for variations in the Earth-Sun distance between consecutive acquisitions (Pacifici et al., 2014). The solar correction removes the influence of solar radiation on pixel values by converting raw DN to TOA reflectance (Young et al., 2017). Equation (1) was utilized in this research to convert the Level 1 DN values of Landsat-8 images to TOA reflectance.

$$\rho'_\lambda = M_\rho * Q_{cal} + A_\rho \quad (1)$$

Where, $\rho\lambda'$ = TOA planetary spectral reflectance, without correction for solar angle (unit less); M_ρ = Reflectance multiplicative scaling factor for the band; A_ρ = Reflectance additive scaling factor for the band; Q_{cal} = Level 1 pixel value in DN

The true TOA reflectance which accounts for solar elevation angle was calculated by equation (2).

$$\rho_\lambda = \frac{\rho'_\lambda}{\cos(\theta_{SZ})} = \frac{\rho'_\lambda}{\sin(\theta_{SE})} \quad (2)$$

Where, ρ_λ = TOA planetary reflectance; θ_{SE} = Local sun elevation angle; θ_{SZ} = Local solar zenith angle; θ_{SZ} =90°- θ_{SE}

c) Atmospheric Correction

The energy reflected and recorded by Landsat sensor is subject to the influence of atmosphere. Atmospheric correction is essential to account for the effects of scattering and absorption, primarily resulting from the interactions between electromagnetic radiation and atmospheric particles (Young et al., 2017). The dark object subtraction (DOS) method is simple and most used in preprocessing of Landsat images. Using the Semi-Automatic Classification plugin (SCP), the DOS was performed in QGIS to allow for atmospheric adjustment.

d) Topographic Correction

The effect of illumination owing to slope, aspect, and elevation could have caused variation in surface reflectance of the same object at different positions. The topographic correction was conducted to avoid any such issues. The DEM was utilized to generate slopes and aspects which were parameters of topographic correction (Young et al., 2017). The in-situ elevation data was surveyed from the field around the reservoir. A new raster topographic map was created by combining field elevation data with a 30m*30m SRTM-DEM. This new raster map was used in topographic correction during image preprocessing. The cosine correction method of Civco 1989 was used for topographic correction.

2.3.5 Extraction of Reservoir Surface Area

The use of water indices is a common, easy, and effective method to extract water bodies from non-water land features (Huang et al., 2018). Several water indices were used by different researchers to extract water surface area. The Normalized Difference Water Index (NDWI), Modified Normalized Difference Water Index (MNDWI), and Automated Water Extraction

Index (AWEI) were some of the most frequently used indices. The AWEI was simple, robust, and accurate technique for extracting water surfaces under different environmental conditions relative to MNDWI (Feyisa et al., 2014). The thresholding technique was a crucial activity in extracting water bodies from non-water features. According to Feyisa et al. (2014), the Automated Water Extraction Index for shadow area (AWEI) had an optimum value of zero. This indicated AWEI greater than or equals to zero could be classified as water while the rest were considered non-water. Authors developed two equations for calculating AWEI indices by considering shadow and shadow free areas. Equation (3) is suitable for conditions where shadows are not a primary concern while equation (4) is effective for areas with shadows and/or other dark surfaces.

$$\mathrm{AWEI_{nsh}} = 4 * (\rho_{\mathrm{band3}} - \rho_{\mathrm{band6}}) - 0.25 * \rho_{\mathrm{band5}} + 2.75 * \rho_{\mathrm{band7}} \quad (3)$$

$$\mathrm{AWEI_{sh}} = \rho_{\mathrm{band2}} + 2.5 * \rho_{\mathrm{band3}} - 1.5 * (\rho_{\mathrm{band5}} + \rho_{\mathrm{band6}}) - 0.25 * \rho_{\mathrm{band7}} \quad (4)$$

Where, ρ is the reflectance values of spectral bands: band 2 = blue; band 3 = green; band 5 = near infrared; band 6 = shortwave infrared 1; band 7 = shortwave infrared 2

The AWEI index was calculated by QGIS raster calculator using equation (4). Subsequently, the AWEI values were reclassified into two classes by using a thresholding technique with a threshold value of zero: water and non-water.. The reclassified raster was then converted to a shapefile using the polygonise tool in QGIS. The water bodies in the AOI were selected and exported as shape files. The reservoir surface area was then extracted by separating other water bodies within the AOI that were not actually portion of the reservoir. The surface areas of the reservoir for all 16 days were then calculated using the geometry tool in QGIS (Figure 4).

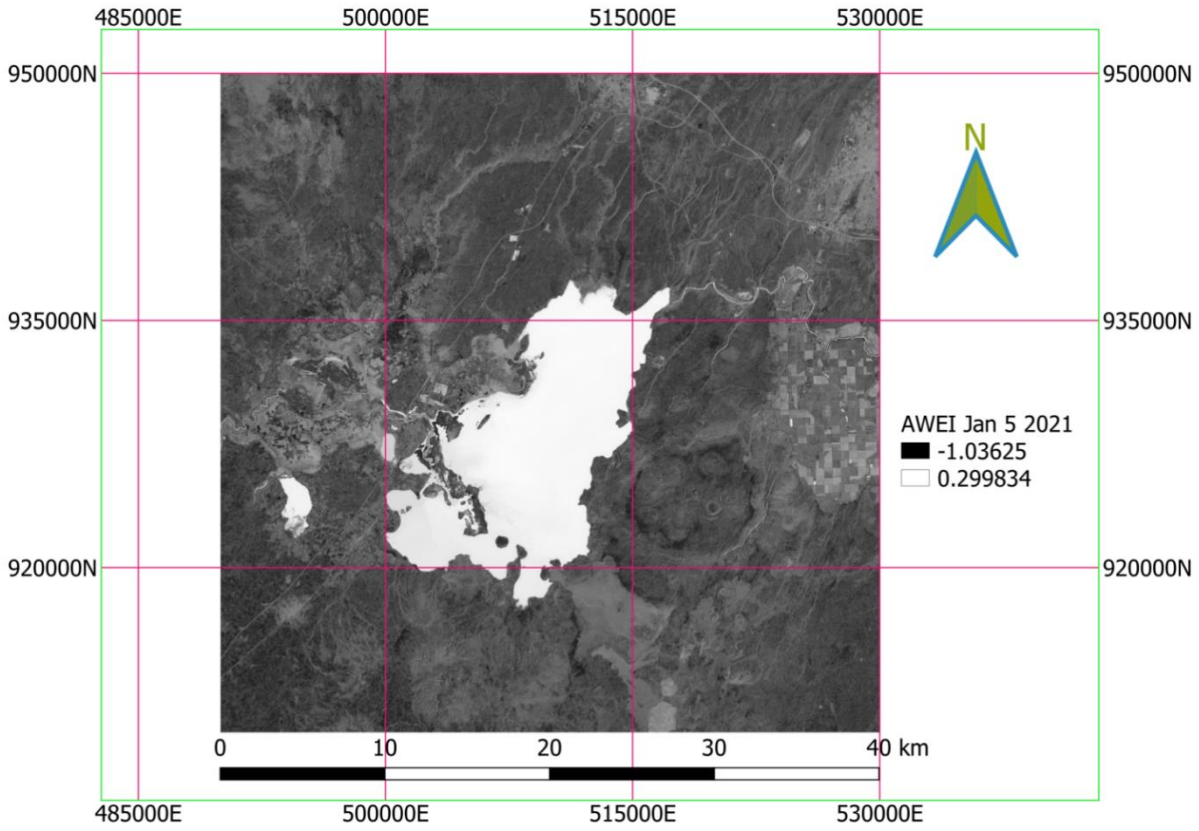

Figure 4 AWEI Value of Landsat-8 OLI Image

2.3.6 Computation of Revised Volume

Several researchers implemented the Prismoidal formula to compute storage capacity of reservoir and prepare a revised capacity curve. For instance, Rathore et al. (2006), Narasayya et al. (2012), Shukla et al. (2017), Rai et al. (2019) and Jeyakanthan et al. (2020) applied the Prismoidal formula to develop a new reservoir volume. For this research, the Prismoidal formula (equation 5) was used to calculate reservoir volume between two consecutive elevations.

$$\Delta V = \frac{\Delta H}{3}\left[A_i + A_j + \sqrt{A_i * A_j}\right] \quad (5)$$

Where, ΔV = Volume between two consecutive elevations; ΔH = Difference between two consecutive elevations; A_i = Reservoir surface area at elevation i; A_j = Reservoir surface area at elevation j.

2.4 Research Design

The technique of extracting necessary information regarding reservoir sedimentation from satellite images has been in use for more than three decades. For instance, satellite image processing technique (Rathore et al., 2006) was utilized to evaluate the sedimentation in the Hirakud and Totla Doh reservoirs of India (Mandwar et al., 2013). Satellite images nurture the origin of water surface area at different elevations of a reservoir to assess the sedimentation in different reservoirs of the world (Shukla et al., 2017; Prasad et al., 2018; Rai et al., 2019, Jeyakanthan et al., 2020; Wagh & Manekar, 2021). The estimated water surface area helps to compute a new reservoir volume and develop a revised elevation-capacity curve. This revised elevation-capacity curve can be compared with the previous survey to assess the volume of reservoir lost because of sedimentation (Figure 5).

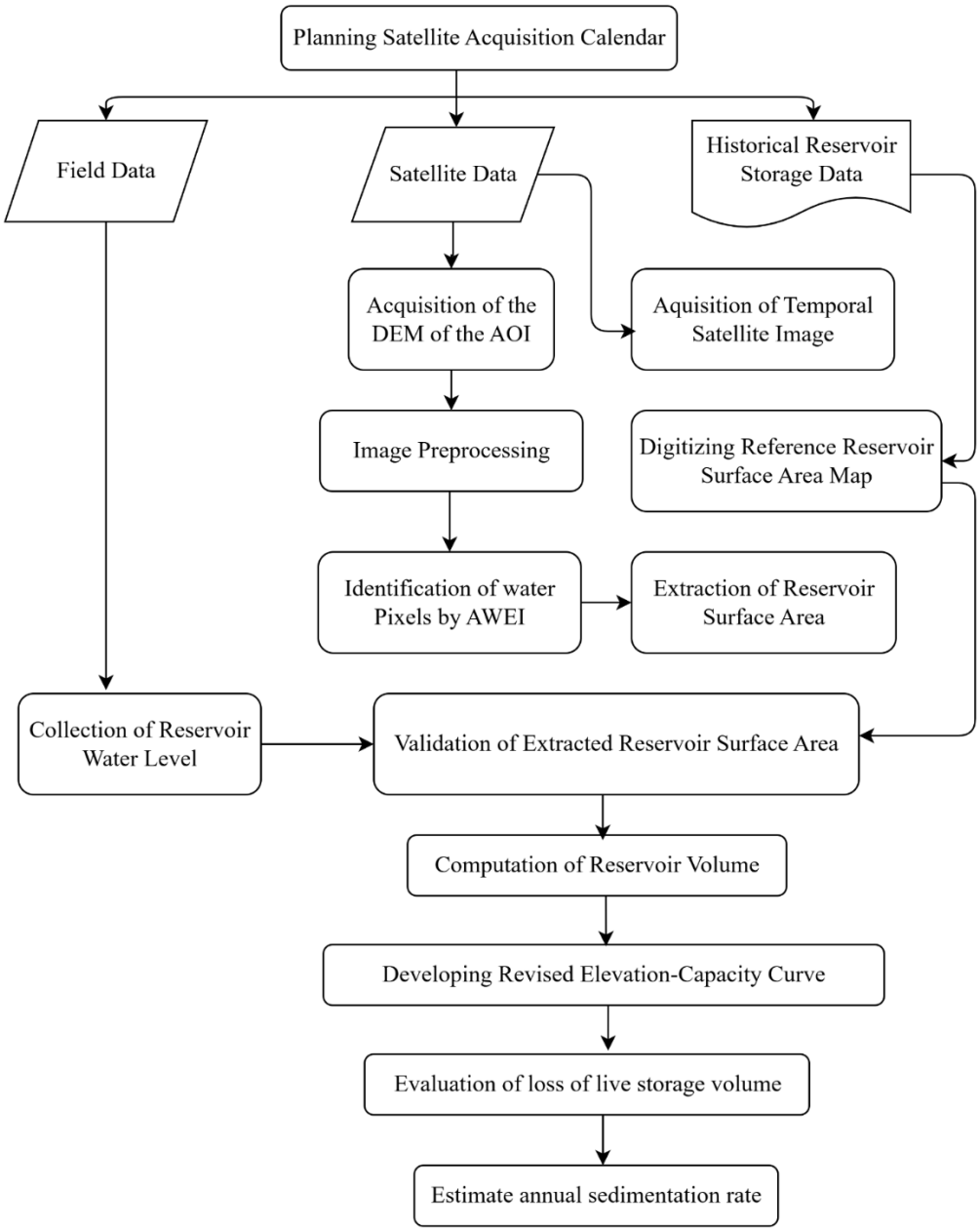

Figure 5 Sequential flow chart of the research

where DEM = Digital Elevation Model, AOI = Area of Interest, GCP = Ground Control Point, AWEI = Automated Water Extraction Index

3 RESULTS AND DISCUSSIONS

3.1 Spatiotemporal Variation of Reservoir Surface Area

The analysis of the reservoir surface area derived from the satellite image series, as depicted in Figure 6, revealed insightful spatiotemporal dynamics. Figure 7 illustrates the relationship

between the reservoir area and the corresponding in-situ reservoir level measurements. Notably, observations showed that the reservoir level tends to approach full capacity during the months of September to November while it typically reaches its minimum operating level from April to June. On June 14, 2021, the satellite data recorded the minimum reservoir surface area of 71.029 km² at a reduced level of 104.11m. Conversely, on October 20, 2021, the maximum observed reservoir area peaked at 157.341 km², corresponding to an elevation of 110.34m. The significant spatiotemporal dynamics between these two periods amounted to 86.312 km².

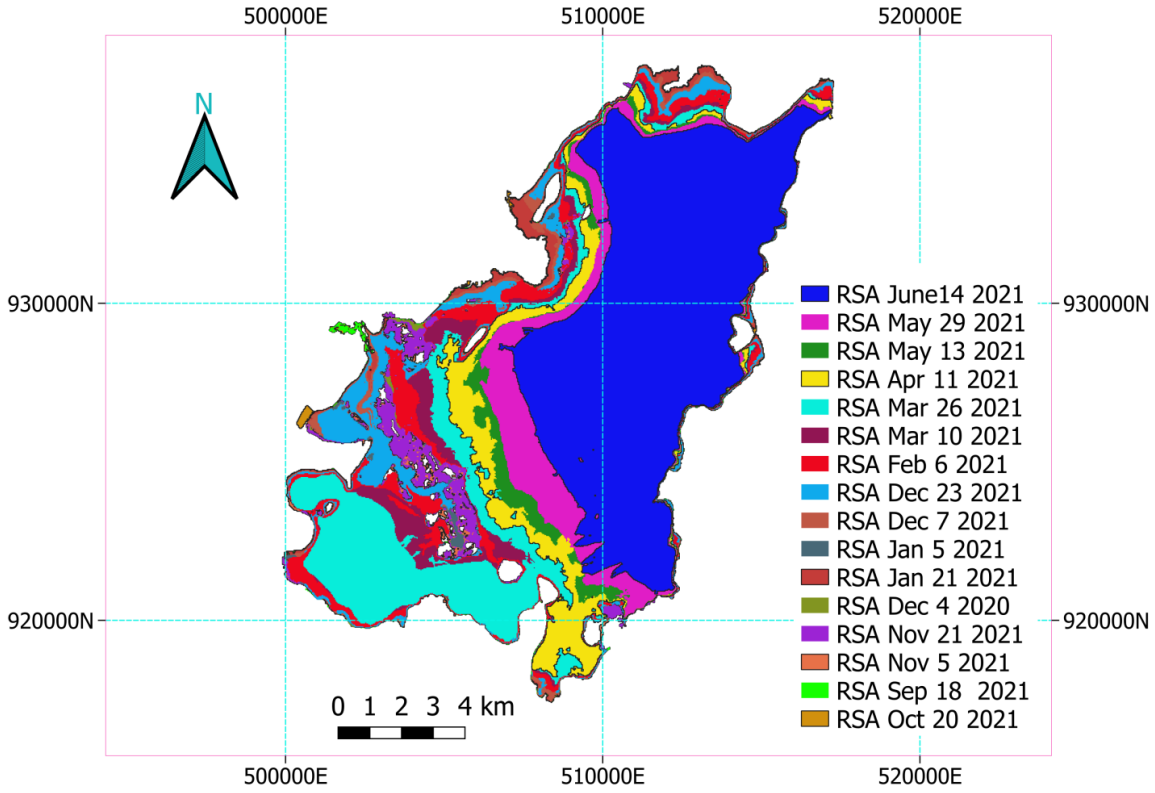

Figure 1 Spatiotemporal dynamics of reservoir area

3.2 Validation of Satellite Derived Reservoir Surface Area

The minimum observed reservoir level during the study period (104.11m) as shown in Figure 7 closely aligned with the minimum operating level estimated during the 2015 survey (103.6m). Similarly, the maximum observed reservoir level during the study (110.34m) was almost equivalent to the full reservoir level (110.3m). This alignment suggested that the fluctuations in reservoir level adequately captured the operational range between the minimum operating level and full reservoir level during the study period. Hence, the remaining storage capacity,

capacity loss to sedimentation, and annual siltation rate within the live storage zone could be quantified with minimal uncertainty. These findings confirmed the reliability and accuracy of utilizing satellite imagery and in-situ reservoir level data for assessing reservoir surface dynamics and sedimentation rate.

Further validation of the satellite-derived surface area was carried out by digitizing the reservoir area map from the 1999 survey and comparing the results at corresponding elevations, as illustrated in Figure 8. The two datasets showed good agreement with only minor deviations at certain elevation points. The analysis yielded a mean absolute error of 5.34 km² and a mean absolute percentage error of 4.57%. This corresponded to an overall accuracy of 92.43%, confirming that the satellite-derived surface area closely matched the digitized dataset and could be reliably used for reservoir volume estimation. The peak reservoir area of 157.341 at an elevation of 110.34 m in October was primarily due to the culmination of the main rainy season inflows and the bathymetric characteristics of the reservoir.

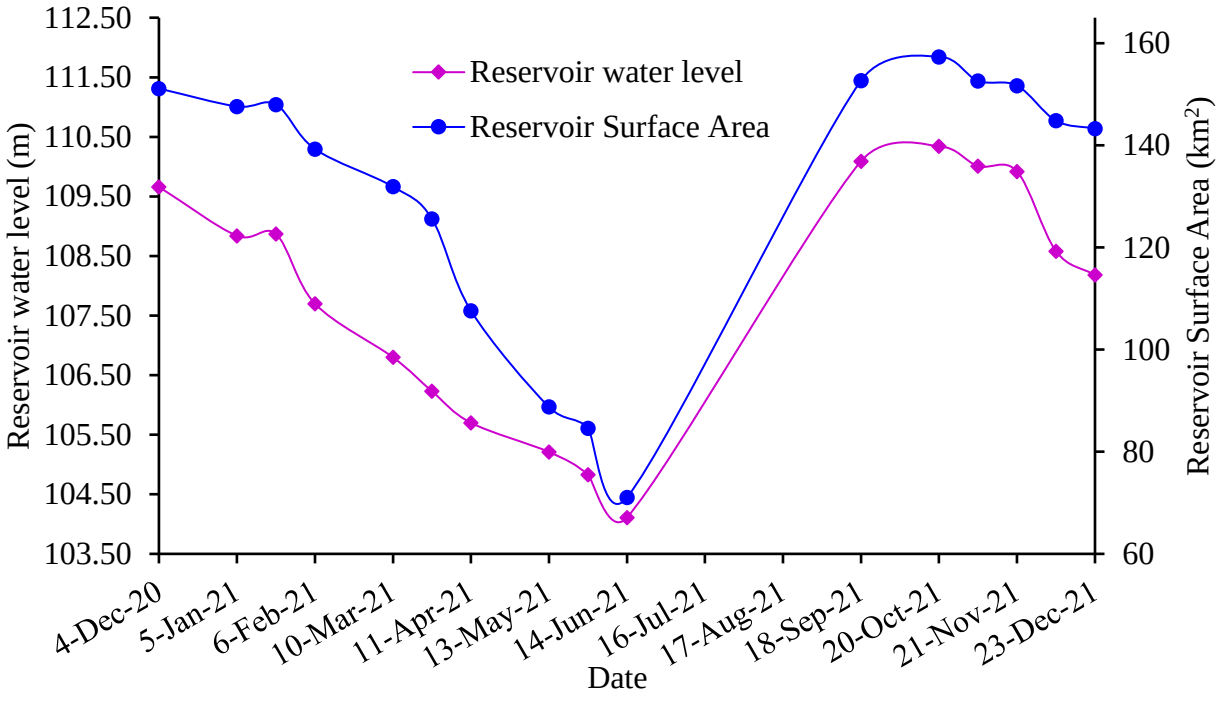

Figure 2 Spatiotemporal dynamics of reservoir area and water level

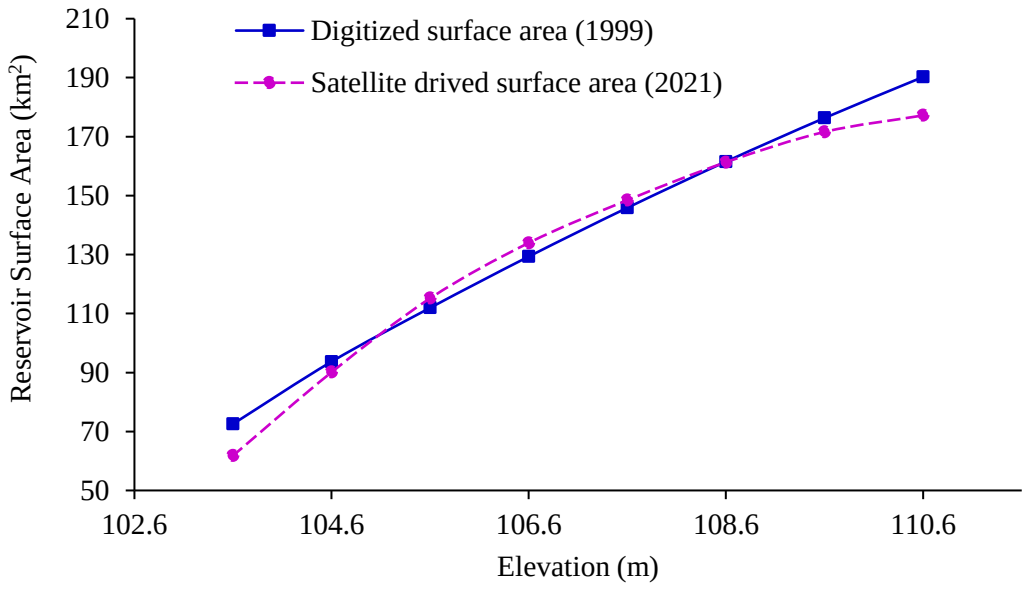

Figure 8 Comparison of satellite derived and digitized reservoir surface area

3.3 Revised Reservoir Storage Capacity Curve

The reservoir surface area, extracted from multidate satellite image, was arranged in ascending order. To calculate a new reservoir storage capacity, this area was paired with the in-situ reservoir elevation data collected on the satellite pass date. Finally, a new elevation-capacity curve was developed (Figure 9).

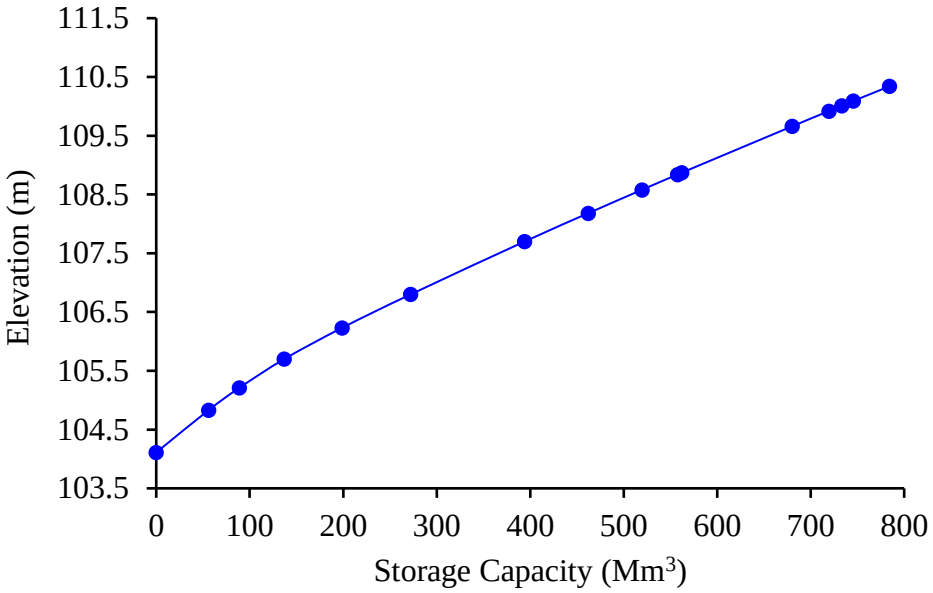

Figure 9 A new elevation-capacity curve derived from satellite image

3.4 Bathymetric Differencing

The previous reservoir survey reports presented the relationship between elevation and storage capacity at equal interval of 1m. However, the current research observed reservoir elevations at irregular intervals. Consequently, performing bathymetric differencing and comparing the present reservoir storage capacity with previous reports was not considered. To address this, a polynomial curve fitting approach was employed to formulate an equation for the elevation-capacity relationship of the Koka Reservoir (Figure 10). This approach facilitated a more convenient method for calculating a new reservoir capacity at elevations like those of previous surveys. It aided the process of conducting bathymetric differencing, enabling a more efficient comparison between the current and historical storage capacities of the reservoir.

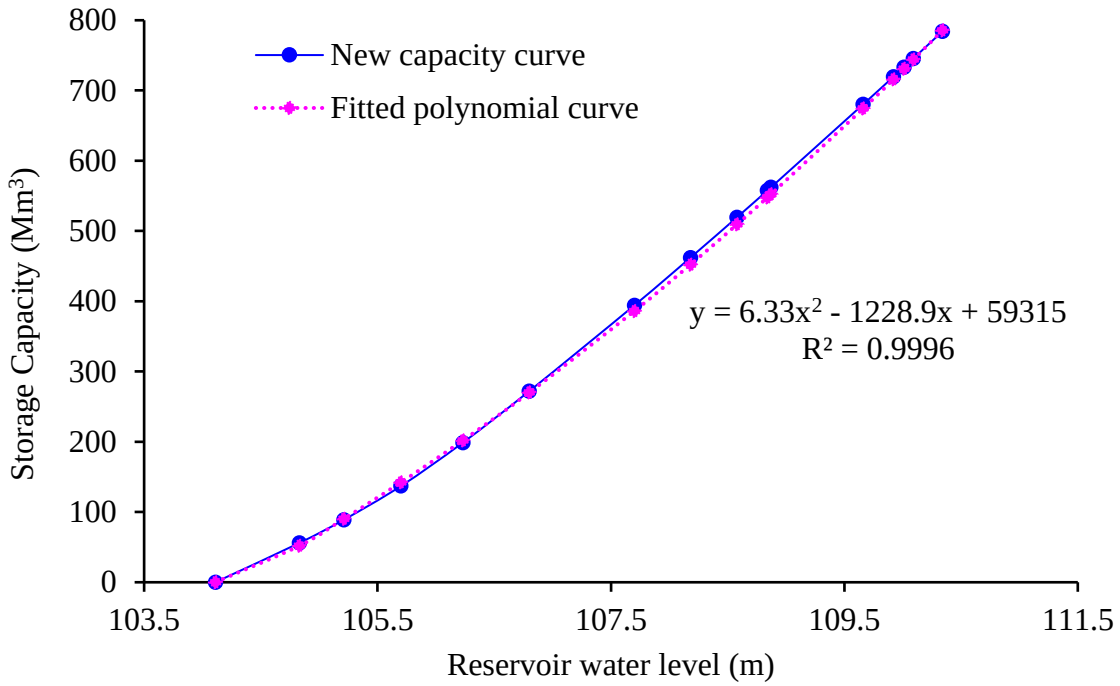

Figure 10 Curve fitted to Elevation-Capacity curve

The bathymetric difference between the new and previous storage capacities at similar elevations disclosed the extent of reservoir sedimentation. The Koka Reservoir storage capacity at full reservoir level (110.3m) was initially 1650 Mm^3 in the year 1959. However, subsequent bathymetric surveys revealed a notable reduction in storage volume over the years. The result of 1999 bathymetric survey indicated that the storage volume was reduced to 1186 Mm^3 at the same level, and by 2015, it further decreased to 978.73 Mm^3. The findings of this research indicated that at the end of December 2021, the Koka Reservoir had a storage capacity of

780.01 Mm³ at full reservoir level. This continuous decline implied that only 47.27% of the original active storage capacity remained available for further use, highlighting the severe impact of sedimentation on functionality of the reservoir and water availability. Figure 11 illustrates the change in the elevation-capacity curve over the past 62 years while Figure 12 presents the decreasing trend of live storage capacity at full reservoir level over the service period of the reservoir. The illustrations provide a convincing narrative of the ongoing challenges faced by the Koka Reservoir. This suggested the urgent need for practical sedimentation management strategies to ensure sustainable water resource management and reservoir operation in the face of increasing sedimentation rates.

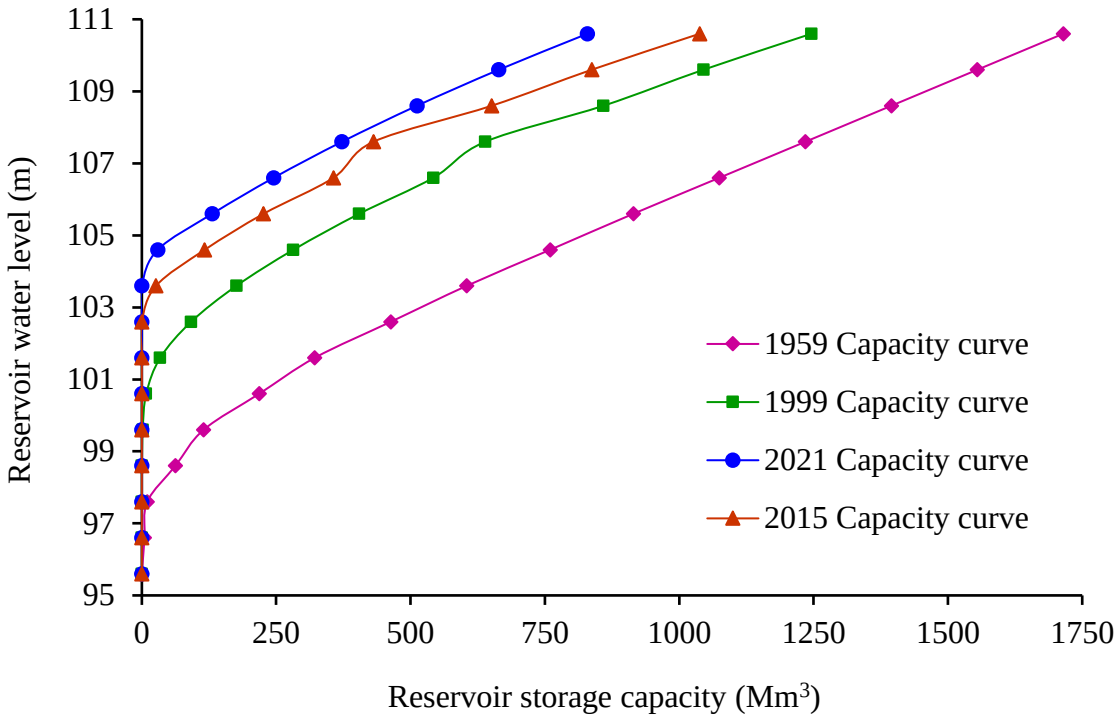

Figure 11 Elevation-Capacity curve of Koka reservoir

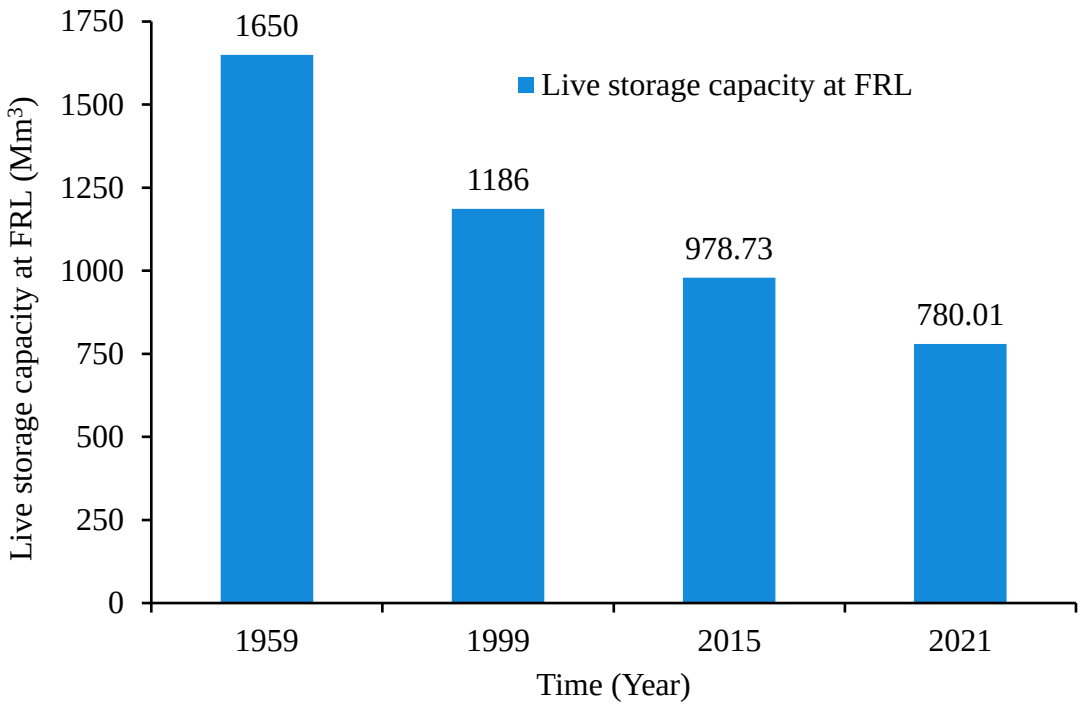

Figure 12 Storage capacity of Koka at full reservoir level

3.5 Estimation of Reservoir Sedimentation

Observations were made to show the trend of sedimentation at the Koka Reservoir over four distinct timeframes: 1959-1999, 1999-2015, 2015-2021, and 1959-2021. According to the 1999 hydrographic survey report, 470Mm^3 of silt was accumulated in the Koka Reservoir between 1959 and 1999. The 2015 report further indicated a volume of 207.27Mm^3 was lost by sedimentation from 1999 to 2015. The current findings revealed that 198.72Mm^3 of reservoir volume was lost because of sedimentation between 2015 and 2021. Overall, the bathymetric differencing between the year 1959 and 2021 showed that 869.99Mm^3 of sediment was deposited in the Koka Reservoir.

These results indicated that over the first 40 years of operation (1959–1999), 28.48% of the original active storage volume was lost. Subsequently, in the following 16 years (1999-2015), the live storage volume observed during the 1999 survey was further reduced by 17.48% (Steyaert and Condon, 2022). Similarly, over the last six years (2015–2021), the live storage capacity in 2015 dropped by 20.30%. Overall, the findings demonstrated that throughout the past 62 years (1959–2021), sedimentation caused the loss of 52.73% of the original active storage capacity. This substantial reduction in reservoir storage volume showed a significant challenge posed by sedimentation on the Koka Reservoir and its escalating impact on

operational life span of the reservoir. The percentage of live storage volume lost owing to sedimentation over the four timeframes is illustrated in Figure 13.

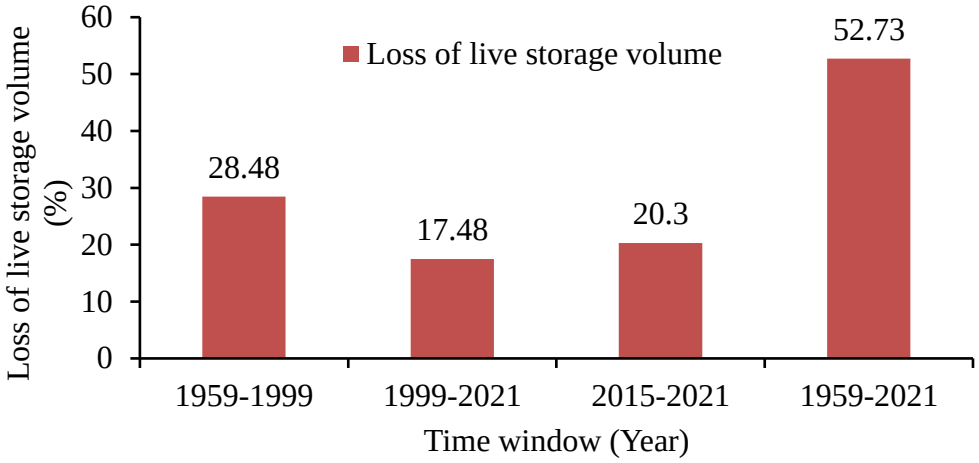

Figure 13 Percentage of reservoir loss

3.6 Rate of Sediment Deposition

The reported average annual rate of sediment deposition from 1959 to 1999 was 12.2Mm³, and it increased to 13Mm³ between 1999 and 2015. The current study identified that the long-term annual rate of sediment deposition from 1959 to 2021 was 14.03Mm³. The results provided valuable insights into the progressive nature of sedimentation in the Koka Reservoir. The observed annual rate of sedimentation showed agreement with previous local studies conducted by Ministry of Water and Energy (1999) and Awash Basin Authority (2015). The current results indicated that the annual percentage of volume loss owing to sedimentation over the past 62 years (1959-2021) was estimated to be 0.85%. The finding of the current study was comparable to the annual global index of reservoir loss because of sedimentation indicated by Merina et al. (2016); Pandey et al. (2016) and Garg et al. (2020). The previous studies of these authors stated that a global annual loss of the existing volume of reservoirs because of sedimentation was estimated to be between 0.5 to 1%. Moreover, the similarity between the findings of these researches and those of Rahamani et al. (2018) and Singh et al. (2023) emphasized the consistency of reservoir depletion rates across different studies. The observed annual depletion rate in this research (0.85%) aligned closely with their reports: 0.84% and 0.58%, respectively. This consistency strengthened the validity of the current results and suggested a general trend in annual reservoir depletion rates.

3.7 Implication of the Upper Awash Flow on Sedimentation Management

The 22-year long-term average (1990-2011) discharge of the Upper Awash River at Hombolle station was analyzed to identify the best timing for reservoir flushing. This was important for reducing the impact of sediment deposition.

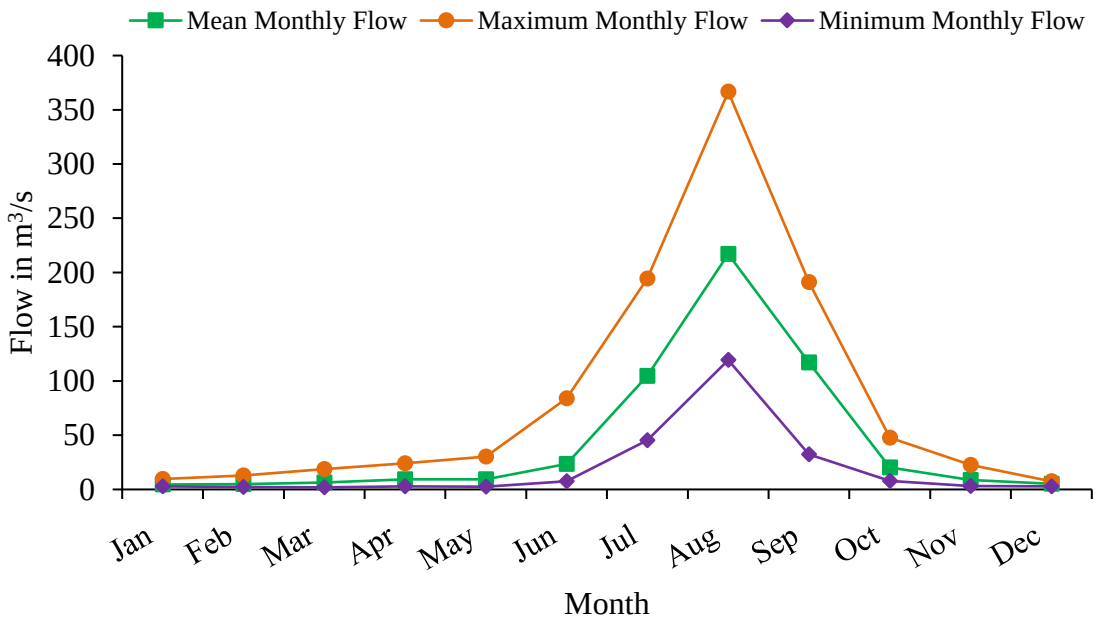

Figure 14 Long term average monthly flow of upper Awash at Hombole

As shown in Figure 14, the river flow was highly seasonal. Very low discharges occurred from November to May, followed by a sharp increase beginning in June. Peak flows were observed in August, reaching more than 350 m³/s. The flow then declined rapidly from September onwards.

This clear seasonality created an opportunity for effective sediment management. The peak flood months, i.e. July to September, coincided with the period when the river had its maximum transport capacity. By aligning flushing operations with this natural flood season, sediment removal efficiency could be maximized. This adaptive management strategy highlighted the importance of integrating long-term hydrological records in planning reservoir flushing operation.

4 CONCLUSION

The observed spatiotemporal fluctuations of the reservoir surface area and water level captured the entire live storage zone, indicating the effectiveness of the new elevation-capacity curve derived from satellite data. The bathymetric differencing highlighted a dramatic reduction in storage volume from 1650 Mm^3 in 1959 to 780.01 Mm^3 in 2021, indicating that only 47.27% of the original live storage capacity remained for further use. The study also indicated a progressive increase in the annual rate of sediment deposition currently at 14.03 Mm^3 per year. The annual depletion rate is also 0.85%, which aligns with global trends. The comprehensive analysis of the Koka Reservoir by integrating multi-date Landsat-8 OLI satellite imagery with real-time reservoir water level data yielded significant insights into its spatiotemporal dynamics, sedimentation status, and overall storage capacity trends. These findings emphasized the escalating impact of sedimentation on the reservoir and water availability. Overall, integrating satellite imagery with in-situ reservoir level data remained a valuable tool for updating elevation-storage curves for reservoir sedimentation assessment, particularly for those seeking rapid and economical solutions. This approach would aid reservoir water allocators in making timely and informed decisions to ensure sustainable water resource management. The flow regime of the Upper Awash indicated that flushing should be carried out during the short but intense flood season, particularly in August and early September. Scheduling sediment management during this period would be a sustainable way to reduce reservoir sedimentation, extend the lifespan of the reservoir, and maintain storage capacity. Synchronizing satellite data with field measurements for thee Koka Reservoir would allow for targeted, season-specific, and cost-effective sediment management. Practical recommendations included using pre-monsoon high-resolution satellite imagery to identify erosion hotspots, implementing upstream conservation during dry seasons, and scheduling reservoir flushing based on peak inflow.

Conflict of Interest Statement

On behalf of all authors, the corresponding author states that there is no conflict of interest.

Funding

This study was funded by the Water Resources Research Centre (WRRC) of Arba Minch University under Project Code GOV/AMU/TH27/AWTI/WRRC/16/2013. However, the authors did not receive support from any other organization.

Data Availability Statement

Data will be available from the corresponding author on request.

REFERENCES

Adugna, T. M., & Cherie, D. A. (2021). A Review on Reservoirs Sedimentation Problems in Ethiopia. Asian Journal of Advanced Research and Reports, 15(3), 1-8. doi:10.9734/AJARR/2021/v15i330372

Al Balasmeh, O. I., Karmaker, T., & Babba, R. (2020). Estimation of Reservoir Capacity and Sediment Deposition Using Remote Sensing Data. World Environmental and Water Resources Congress (pp. 154-161). ASCE. doi:10.1061/9780784482957.016

Chamoun, S., De Cesare, G., & Schleiss, A. J. (2016). Managing reservoir sedimentation by venting turbidity currents: A review. International Journal of Sediment Research, 31(4), 195-204. doi:10.1016/j.ijsrc.2016.06.001

Ethiopian Electric Power Corporation. (2004). Facts About Power Plants in Brief. Addis Abeba: Ethiopian Electric Power Coorporation.

European Space Agency. (2020, August 28). Sentinel Online. Retrieved August 28, 2020, from https://sentinel.esa.int/web/sentinel/user-guides/sentinel-2-msi/overview

Feyisa, G. L., Meilby, H., Fensholt, R., & Proud, S. R. (2014). Automated Water Extraction Index: A new technique for surface water mapping using Landsat imagery. Remote Sensing of Environment, 140, 23-35. doi:10.1016/j.rse.2013.08.029

Fitensa, T., Biedebrhan, M., & Simachew, S. (2019). Hydrologic and Structural Safety Evaluation of Aged Concrete Gravity Dam Using Finite Element Method. American Journal of Water Science and Engineering, 5(4), 138-154. doi:10.11648/j.ajwse.20190504.12

Garg, A. A., Shawul, A. A., & Chakma, S. (2020). Assessment of sedimentation and useful life of Tehri reservoir using integrated approaches of hydrodynamic modeling, satellite remote sensing and empirical curves. Current Science, 118(3), 411-420. doi:10.18520/cs/v118/i3/411-420

Huang, C., Chen, Y., Zhang, S., & Wu, J. (2018). Detecting, Extracting, and Monitoring Surface Water From Space Using Optical Sensors: A Review. Reviews of Geophysics, 56(2), 333-360. doi:10.1029/2018RG000598

Jain, S. K., & Jain, S. K. (2011). Assessment of Reservoir Sedimentation Using Remote Sensing. Sediment Problems and Sediment Management in Asian River Basins (Proceeding of workshop) (pp. 163-170). Hyderabad: IAHS Press.

Jeyakanthan, V. S., Phanindra, C., Rao, P. S., & Venkataramana, R. (2020). Sedimentation assessment of Hirakud reservoir using Microwave Remote sensing Technology. International Conference on Recent Development in Engineering Sciences, Humanities and Management , (pp. 88-98). Bharatpur.

Khadatare, M. Y., & Jedhe, S. H. (2017). Sediment Assessment of UJJANI Reservoir in Maharashtara by Using Remote Sensing Technique. International Research Journal of Engineering and Technology, 4(8), 1255-1258.

Mandwar, S. R., Hajare, H. V., & Gajbhiye, A. R. (2013). Assessment of Capacity Evaluation and Sedimentation of Totla Doh Reservoir, In Nagpur District by Remote sensing Technique. IOSR Journal of Mechanical and Civil Engineering, 4(6), 22-25. doi:10.9790/1684-0462225

Merina, N., Shashikkumar, R., Rizvana, M. C., & R., N. A. (2016). Sedimentation Study in A Reservoir Using Remote Sensing Technique. Applied Ecology and Environmental Research, 14(4), 296-304. doi:10.15666/aeer/1404_296304

Ministry of Water and Energy. (1999). Koka Hydrographic Survey Report.

MupFiga, E. T., Munkwakwata, R., Mudereri, B., & Nyatondo, U. N. (2016). Assessment of Sedimentation in Tuli-Makwe Dam Using Remotely Sensed Data. Journal of Soil Science and Environmental Management, 7(12), 230-238. doi:10.5897/JSSEM2016.0563

Narasayya, K., Roman, U. C., Sreekanth, S., & Jatwa, S. (2012). Assessment of Reservoir Sedimentation Using Remote Sensing Satellite Imageries. Asian Journal of Geoinformatics, 12(4), 1-8.

Pacifici, F., Longbotham, N., & Emery, W. J. (2014). The Importance of Physical Quantities for the Analysis of Mult Spatiotemporal and Multiangular Optical Very High Spatial Resolution Images. IEEE TRANSACTIONS ON GEOSCIENCE AND REMOTE SENSING, 52(10), 6241-6256. doi:10.1109/TGRS.2013.2295819

Pandey, A., Chaubey, U. C., Mishra, S. K., & Kumar, D. (2016). Assessment of reservoir sedimentation using remote sensing and recommendations for desilting Patratu Reservoir, India. Hydrological Sciences Journal, 61(4), 711-718. doi:10.1080/02626667.2014.993988

Prasad, N. R., Garg, V., & Thakur, P. K. (2018). The Role of SAR Data in Water Body Mapping and Reservoir Sedimentation Assessment. Geospatial Technology– Pixel to People. IV-5, pp. 151-158. Dehradun: ISPRS Annals of the Photogrammetry, Remote Sensing and Spatial Information Sciences. doi:10.5194/isprs-annals-IV-5-151-2018

Rahamani, V., Kastens, J. H., DeNoyelles, F., Jakubauskas, M. E., Martinko, E. A., Huggins, D. H., Blackwood, A. J. (2018). Examining Storage Capacity Loss and Sedimentation Rate of Large Reservoirs in the Central U.S. Great Plains. Water, 1-17.

Rai, A. K., Jaiswal, R. K., Galkate, R., & Nayak, T. R. (2019). Assessment of Sedimentation in Kharkhara and Paralkot Reservoir using Digital Image Processing Techniques. International Journal of Advance and Innovative Research, 6(2), 162-169.

Rathore, D. S., Choudhary, A., & Agarwal, P. K. (2006). Assessment of Sedimentation in Harakud Reservoir using Digital Remote Sensing Technique. Journal of the Indian Society of Remote Sensing, 377-383.

REACH (2020) Report on findings from the Awash River basin. Mid Programme Synthesis. University of Oxford, Oxford, UK.

Shukla, S., Jain, S. K., Kansal, M. L., & Chandniha, S. K. (2017). Assessment of sedimentation in Pong and Bhakra reservoirs in Himachal Pradesh, India, using geospatial technique. Remote Sensing Applications:Society and Environment, 8(4), 148-156. doi:10.1016/j.rsase.2017.08.008

Singh, M. C., Prashar, A., Singh, J., & Kumar, S. (2023). Reservoir capacity loss and sedimentation assessment of Dholbaha dam located in Punjab, India using remote sensing and bathymetric survey techniques. Water Practice & Technology, 2901–2922.

Steyaert, J. C. and Condon, L. E. (2022). Historical Analysis of Reservoir Storage Trends and Resilience Across Contiguous US from 1980–2019, EGUsphere [preprint], https://doi.org/10.5194/egusphere-2022-1051.

Tawfeik, M., Elhifnawy, H., Hamza, E., & Shawky, A. (2016). Determination of suitable requirements for Geometric Correction of remote sensing Satellite Images when Using Ground Control Points. International Research Journal of Engineering and Technology (IRJET), 3(10), 54-62.

Tiwari, S., Verma, S., & Ghosh, S. (2016). Estimation of Sedimentation Rate of a Reservoir using Remote Sensing Data: a case study of Tehri Reservoir. International Journal of Latest Trends in Engineering and Technology, 7(3), 245-253. doi:10.21172/1.73.034

United States Geological Survey. (2020, August 24). U.S. Geological Survey. Retrieved August 24, 2020, from https://www.usgs.gov/land-resources/nli/landsat/landsat-8

Wagh, S., & Manekar, V. (2021). Assessment of Reservoir Sedimentation using Satellite Remote Sensing Technique (SRS). Journal of The Institution of Engineers (India): Series A, 102(3), 851–860. doi:10.1007/s40030-021-00539-8

Young, N. E., Anderson, R. S., Chignell, S. M., Vorster, A. G., Lawrence, R., & Evangelista, P. H. (2017). A Survival Guide to Landsat Preprocessing. Ecology, 98(4), 920-932. doi:10.1002/ecy.1730

Zhou, T., Gao, H., & Lettenmaier, D. (2016). The contribution of reservoirs to global land surface water storage variations. Journal of Hydrometeorology, 17(1), 309-325. doi:10.1175/JHM-D-15-0002.1